

# THE GREEN BANK TELESCOPE MAPS THE DENSE, STAR-FORMING GAS IN THE NEARBY STARBURST GALAXY M82

AMANDA A. KEPLEY

National Radio Astronomy Observatory, P.O. Box 2, Green Bank, WV 24944-0002

ADAM K. LEROY

National Radio Astronomy Observatory, 520 Edgemont Road, Charlottesville, VA 22903-2475

DAVID FRAYER

National Radio Astronomy Observatory, P.O. Box 2, Green Bank, WV 24944-0002

ANTONIO USERO

Observatorio Astronómico Nacional, C/ Alfonso XII, 3, E-28014 Madrid, Spain

JOSH MARVIL

Department of Physics, New Mexico Tech., 801 Leroy Place, Socorro, NM 87801, USA ; National Radio Astronomy Observatory, P.O. Box O, 1003 Lopezville Road, Socorro, NM 87801, USA

FABIAN WALTER

Max Planck Institute für Astronomie, Königstuhl 17, D-69117 Heidelberg, Germany

*Draft version November 9, 2018*

## ABSTRACT

Observations of the Milky Way and nearby galaxies show that dense molecular gas correlates with recent star formation, suggesting that the formation of this gas phase may help regulate star formation. A key test of this idea requires wide-area, high-resolution maps of dense molecular gas in galaxies to explore how local physical conditions drive dense gas formation, but these observations have been limited because of the faintness of dense gas tracers like HCN and HCO<sup>+</sup>. Here we demonstrate the power of the Robert C. Byrd Green Bank Telescope – the largest single-dish millimeter radio telescope – for mapping dense gas in galaxies by presenting the most sensitive maps yet of HCN and HCO<sup>+</sup> in the starburst galaxy M82. The HCN and HCO<sup>+</sup> in the disk of this galaxy correlates with both recent star formation and more diffuse molecular gas and shows kinematics consistent with a rotating torus. The HCO<sup>+</sup> emission extending to the north and south of the disk is coincident with the outflow previously identified in CO and traces the eastern edge of the hot outflowing gas. The central starburst region has a higher ratio of star formation to dense gas than the outer regions, pointing to the starburst as a key driver of this relationship. These results establish that the GBT can efficiently map the dense molecular gas at 90 GHz in nearby galaxies, a capability that will increase further with the 16 element feed array under construction.

*Subject headings:* galaxies: individual (M82) — ISM: molecules — galaxies: ISM — galaxies: starburst — galaxies: star formation — radio lines: ISM

## 1. INTRODUCTION

Observations of local Milky Way clouds show that the bulk of molecular gas is inert with star formation concentrated in the small fraction of the cloud at high surface density (Heiderman et al. 2010; Lada et al. 2010, 2012). This observation leads to the idea that the “dense” molecular gas ( $A_V \gtrsim 10$  mag,  $n(H_2) \gtrsim 10^4$  cm<sup>-3</sup>), rather than the whole molecular interstellar medium ( $A_V \gtrsim 1$  mag,  $n(H_2) \gtrsim 10^2$  cm<sup>-3</sup>), represents the star-forming phase.

Extragalactic scaling relations also support the idea that the amount of high density molecular gas helps to set the star formation rate. Low angular resolution

spectroscopy of nearby galaxies reveal a constant ratio (within a factor of a few) of HCN intensity, which traces the mass of dense gas, to infrared (IR) emission, which traces the rate of recent star formation, across a wide range of systems, including the central parts of nearby disks, starbursts, and major mergers (Gao & Solomon 2004b; Juneau et al. 2009; García-Burillo et al. 2012). Surprisingly, the HCN-to-IR ratios for whole galaxies are comparable to those in local cloud cores (Wu et al. 2010), implying a constant ratio of dense gas to star formation rate. The ratios of CO intensity, which trace the overall molecular gas mass, to the IR emission, however, vary by more than a factor of ten between disk and starburst galaxies, suggesting that in extreme regions the relationship between the total molecular gas mass and

the amount of star formation may be non-linear (Gao & Solomon 2004b; Leroy et al. 2013; Carilli & Walter 2013).

If the amount of dense gas is linked to the amount of star formation, then the formation of dense gas from more diffuse molecular gas represents an important regulating process. While there may be many regulating steps (e.g., the formation of giant molecular clouds out of diffuse HI, accretion onto the galaxy), differences among density probability distribution functions (PDFs) of local clouds (Kainulainen et al. 2009) and the contrast between ULIRGs, LIRGs, and normal spirals (García-Burillo et al. 2012, Usero et al., in prep.) support the idea that the ratio of dense to total molecular gas varies in different environments.

This hypothesis can be tested in nearby galaxies by comparing dense gas, as traced by HCN and  $\text{HCO}^+$ , to the total molecular gas, as traced by CO. While observations of nearby galaxies have lower spatial resolution and sensitivity than observations in the Milky Way, nearby galaxies probe a wider range of physical conditions than found in the Solar Neighborhood and more directly relate positions with environmental conditions. The main obstacle to pursuing systematic studies of the HCN-to-CO ratio, or analogous measures of the dense gas fraction like the  $\text{HCO}^+$ -to-CO ratio, has been the faintness of the line emission: averaged over a large part of a galaxy, the HCN and  $\text{HCO}^+$  lines are 10–30 times fainter than CO (Gao & Solomon 2004b). As a result, most studies of extragalactic dense gas with small-aperture millimeter-wave telescopes have focused on individual deep pointings rather than wide-field maps. The new  $\lambda \sim 4\text{mm}$  (“W band”) heterodyne receiver on the Robert C. Byrd Green Bank Telescope (GBT) has the potential to extend these single-pointing observations and map HCN and  $\text{HCO}^+$  distributions in nearby galaxies because of the GBT’s large collecting area, high surface accuracy, and good resolution.

In this Letter, we demonstrate the power of the GBT as an HCN and  $\text{HCO}^+$  mapping machine for nearby galaxies using new GBT maps of HCN ( $J = 1 - 0$ ) and  $\text{HCO}^+$  ( $J = 1 - 0$ ) in the nearby ( $D=3.530\text{ Mpc}$ ; Dalcanton et al. 2009) starburst galaxy M82 (Rieke et al. 1980). These observations – from less than 15 hours of telescope time – have the best surface brightness sensitivity of any published HCN or  $\text{HCO}^+$  map of M82 and resolution  $< 200\text{ pc}$ . We compare the HCN and  $\text{HCO}^+$  emission to that of the bulk molecular gas traced by  $^{12}\text{CO}(2 - 1)$  and  $^{12}\text{CO}(1 - 0)$  and to recent star formation traced by 3 GHz radio continuum emission.

## 2. GBT OBSERVATIONS

We used the newly commissioned 4mm (“W band”) receiver and the GBT Spectrometer to simultaneously map the HCN ( $J = 1 - 0$ ) ( $\nu_{rest} = 88.63160\text{ GHz}$ ) and  $\text{HCO}^+$  ( $J = 1 - 0$ ) ( $\nu_{rest} = 89.18853\text{ GHz}$ ) intensity across the central  $1.75'$  by  $1.5'$  ( $1.8 \times 1.5\text{ kpc}$ ) of M82. Table 1 gives the details of the observations (GBT project 13A-253).

We used a single beam of the W-band receiver to make rapid maps, sampling five times each beam FWHM in the scanning direction and sampling 2.4 times each beam FWHM in the orthogonal direction (Mangum et al. 2007).

The observations were made over  $\sim 15\text{h}$  in excellent

weather. Out-of-focus holography scans were made every two hours to correct the dish surface, pointing and focus checks were made every hour, and flux calibration observations were done every observing session. The receiver gain was calibrated using hot and cold loads.<sup>1</sup> The “OFF” spectrum was created using the average of the first and last integrations of each row. We subtracted a linear baseline from each calibrated spectrum and then corrected for the atmospheric opacity using GBT weather models.<sup>2</sup>

The aperture efficiencies ( $\eta_a$ ) were derived using observations of sources from the CARMA CALfind database. CARMA typically measured fluxes at 103.5 GHz, but the difference between 103.5 GHz and 88 GHz flux densities will be only  $\sim 20\%$  even for a steep spectral index ( $F_\nu \propto \nu^{-1}$ ). Applying the derived aperture efficiency to pointing source observations for each observing block yielded consistent flux densities. The structures we observe are comparable to the beam size, so we convert our final maps from  $T'_A$  to  $T_{mb}$  using the main beam efficiency ( $\eta_{mb}$ ), which is  $\approx 1.3\eta_a$  for the GBT (Maddalena 2010). The value of  $\eta_{mb}/\eta_a$  changes by less than 15% for source sizes up to  $60''$  because of the clean nature of the GBT beam (R. Maddalena, priv. comm., 2013).

The calibrated spectra were gridded using a Bessel function tapered by a Gaussian (for details see Mangum et al. 2007). The final cubes have a beam size  $\approx 9.2''$ , slightly larger than the native  $8.3''$  GBT resolution, and were smoothed to a spectral resolution of 3.9 MHz ( $13.2\text{ km s}^{-1}$  for HCN and  $13.14\text{ km s}^{-1}$  for  $\text{HCO}^+$ ). The typical noise per channel ( $T_{mb}$ ) is 42mK (HCN) and 31mK ( $\text{HCO}^+$ ) and each map has  $\sim 100$  independent resolution elements.

We used IRAM 30m HCN observations of M82 from the literature to assess the accuracy of our flux density scale. After smoothing our cube to the resolution of the 30m at 89 GHz ( $28''$ ), we derive an integrated flux of  $28.75 \pm 1.24\text{ K km s}^{-1}$  for the center of M82. This value agrees with 30m HCN integrated fluxes from the literature:  $29\text{ K km s}^{-1}$  (Krips et al. 2008),  $29.9\text{ K km s}^{-1}$  (Fuente et al. 2008),  $27.4\text{ K km s}^{-1}$  (Gao & Solomon 2004a), and  $25.4\text{ K km s}^{-1}$  (Nguyen-Q-Rieu et al. 1989).

## 3. RESULTS

The HCN and  $\text{HCO}^+$  maps demonstrate the GBT’s excellent capabilities for mapping large areas at high surface brightness sensitivity with good resolution (Figure 1). Higher resolution maps have been published for both HCN  $J = 1 - 0$  (Brouillet & Schilke 1993) and  $\text{HCO}^+$   $J = 1 - 0$  (Seaquist et al. 1998), but our maps have better surface brightness sensitivity by a factor of four and cover a larger area.

We compare our maps to lower resolution  $^{12}\text{CO}(2 - 1)$  mapping from the HERACLES survey (Leroy et al., in prep) and to higher resolution, zero-spacing corrected  $^{12}\text{CO}(1 - 0)$  interferometric maps (Walter et al. 2002). The  $^{12}\text{CO}(2 - 1)$  map has  $20.1''$  resolution and covers a wide field. The  $^{12}\text{CO}(1 - 0)$  map has higher resolution ( $3.6''$ ), but covers a smaller field of view. We also compare our data to a new 3.0 GHz Jansky Very Large Ar-

<sup>1</sup> See <http://www.gb.nrao.edu/4mm/>.

<sup>2</sup> <http://www.gb.nrao.edu/rmaddale/Weather/>

TABLE 1  
 SUMMARY OF OBSERVATIONS

	9 March 2013	10 March 2013	21 April 2013
UT Times	3:15 – 11:15	3:45 – 6:45	2:00 – 5:45
Number of Spectral Windows	2	2	2
Bandwidth per Window (MHz)	200	200	200
Spectral Resolution (kHz)	24.414	12.207	12.207
Flux Calibrator	0359+5057	1229+0203	1229+0203
Flux Calibrator Flux (Jy) <sup>a</sup>	4.0 <sup>b</sup>	8.5 <sup>b</sup>	9.9 <sup>c</sup>
Pointing Source	0841+7053	0841+7053	0841+7053
Average Opacity <sup>d</sup>	0.086	0.109	0.082
Average System Temperature (HCN, HCO <sup>+</sup> ) (K)	109, 117	112, 117	89, 88
Main Beam Efficiency (HCN, HCO <sup>+</sup> )	0.26, 0.29	0.26, 0.30	0.23, 0.22 <sup>e</sup>

<sup>a</sup> Values from the CARMA Calfind database (<http://carma.astro.umd.edu/cgi-bin/calfind.cgi>).

<sup>b</sup> At 103.5 GHz.

<sup>c</sup> At 92.6 GHz.

<sup>d</sup> From GBT High Frequency Weather Forecasts (<http://www.gb.nrao.edu/~rmaddale/WeatherNAM/>).

<sup>e</sup> The actuators for a section of panels were inoperational for this session leading to lower efficiencies.

ray (VLA) continuum map (Marvil et al., 2013, in prep), which has  $\approx 0.7''$  resolution and includes a mixture of free-free and synchrotron emission, which both trace the distribution of recent star formation. The total flux in the map agrees with the total flux measured from single dish observations in the literature.

### 3.1. HCN, HCO<sup>+</sup>, and CO comparison

The morphology of HCN and HCO<sup>+</sup> emission follows the galaxy disk and coincides with the main ridge of <sup>12</sup>CO(1 – 0) emission and the star formation traced by the radio continuum emission (top and middle panels of Figure 1). The velocity distributions of the disk HCN and HCO<sup>+</sup> emission are similar to the velocity distribution of the CO disk (bottom panels of Figure 1), suggesting that the HCN, HCO<sup>+</sup>, and CO emission in the disk originates from the same rotating molecular torus (Nakai et al. 1987; Shen & Lo 1995).

For the first time, we also measure HCO<sup>+</sup> emission at low surface brightness associated with the <sup>12</sup>CO(1 – 0) emission extending north and south of the main disk (Walter et al. 2002). Simulations of the GBT beam shape at 4 mm indicate that this emission does not originate from sidelobes. The HCO<sup>+</sup> emission outlines the eastern edge of the X-ray emission associated with the central outflow, suggesting that the dense molecular gas is entrained in the outflow of lower density gas. The HCO<sup>+</sup> in this region also is kinematically inconsistent with a disk, similar to what is seen in CO (cf. Figure 6 in Walter et al. 2002 and Figure 1 here).

CO emission has been associated with the outflow in M82 (Walter et al. 2002) and has been seen in the outflow from the starburst nucleus of NGC 253 (Bolatto et al. 2013). Emission from HCN and HCO<sup>+</sup> has also been associated with the AGN-driven outflow in the ULIRG Mrk 231 (Aalto et al. 2012). To our knowledge, the current observations, however, would be the first time that dense molecular gas, as traced by HCO<sup>+</sup>, has been found to be associated with a starburst-driven outflow in a nearby galaxy. The outflow of dense molecular gas seen in HCO<sup>+</sup> may regulate star formation in galaxies like M82 by removing the fuel for star formation.

The disk-averaged line profiles of the HCN and HCO<sup>+</sup> emission agree with <sup>12</sup>CO(2 – 1) emission from the HERACLES image (Leroy et al., in prep) in Figure 2. Both

HCN and HCO<sup>+</sup> have structure near 220 km s<sup>-1</sup>, which is not seen in <sup>12</sup>CO(2 – 1) but is seen in the higher order CO transitions (Loenen et al. 2010). The models of the CO emission from Loenen et al. (2010) show that the different CO transitions reflect different molecular gas densities. Transitions like <sup>12</sup>CO(2 – 1) are emitted by relatively diffuse ( $10^{3.5}$  cm<sup>-3</sup>) molecular gas associated with the disk, while the higher order CO transitions ( $J > 4$ ) are emitted by two denser components ( $10^5$  cm<sup>-3</sup> and  $10^6$  cm<sup>-3</sup>) associated with the star-forming gas (Loenen et al. 2010). Inspection of the channel maps near 220 km s<sup>-1</sup> confirm that the lack of structure in the <sup>12</sup>CO(2 – 1) is due to the presence of a significant amount of CO emission associated with the warm and diffuse molecular gas found throughout the disk, while the HCN and HCO<sup>+</sup> trace the denser molecular gas component found in the torus.

### 3.2. The Relationship Between HCN, HCO<sup>+</sup>, CO, and Star Formation

To explore the relationships between HCN, HCO<sup>+</sup>, CO, and star formation within M82, we smoothed the images to the same resolution (9.2''), regridded them to the same coordinate system, and rebinned the pixels so that each pixel represents an independent sample. The line intensities were derived from moment zero maps and the luminosities were calculated by multiplying the intensities by the area of a pixel. Regions less than  $3\sigma$  were blanked.

Figure 3 compares the distribution of  $L_{CO}/L_{HCN}$ ,  $L_{CO}/L_{HCO+}$ , and  $L_{HCN}/L_{HCO+}$  for regions within M82 and for entire galaxies (or centers of galaxies) from the literature (Gao & Solomon 2004b; Graciá-Carpio et al. 2008; Juneau et al. 2009; García-Burillo et al. 2012). In M82, the distributions of all three ratios have the same range as the points from the literature, although  $L_{CO}/L_{HCN}$  and  $L_{CO}/L_{HCO+}$  do peak at lower values. However, we must be cautious because we are comparing measurements of entire galaxies with spatially resolved measurements within a galaxy. Because the CO emission has a larger filling factor than the HCN emission, the unresolved measurements may have systematically larger  $L_{CO}/L_{HCN}$  and  $L_{CO}/L_{HCO+}$  ratios. The  $L_{CO}/L_{HCN}$  and  $L_{HCN}/L_{HCO+}$  values for M82 as a whole are sim-

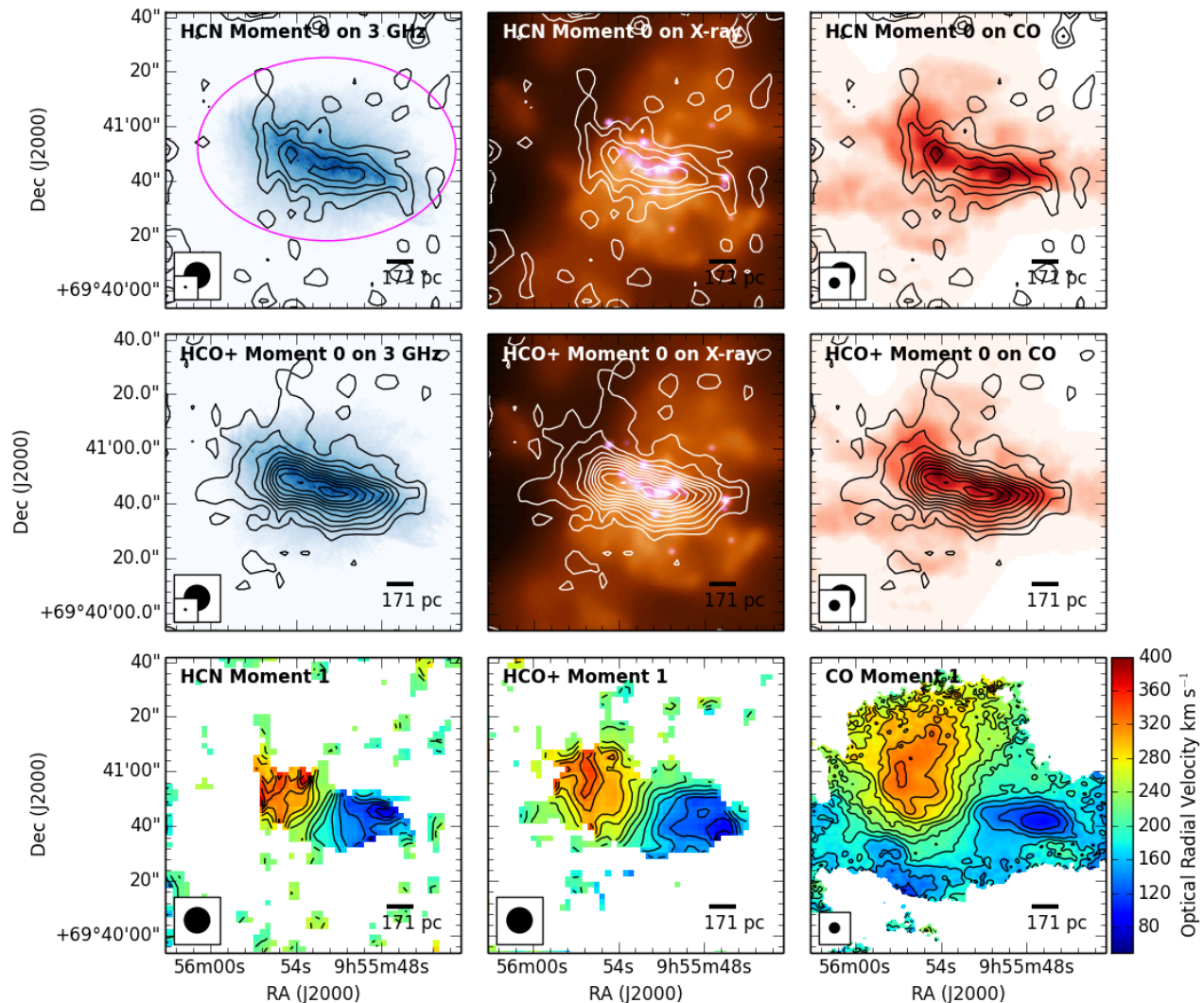


FIG. 1.— *Top and Middle Rows:* The HCN (top) and  $\text{HCO}^+$  (middle) integrated line flux (moment zero) contours overlaid on a 3 GHz radio continuum image (Marvil et al. in prep; left), an X-ray image with the point sources highlighted in pink (NASA/CXC/SAO/PSU/CMU; middle), and a  $^{12}\text{CO}(1-0)$  integrated flux image (Walter et al. 2002; right). The HCN and  $\text{HCO}^+$  emission are both correlated with the total molecular gas and star formation in the center of M82. The diffuse  $\text{HCO}^+$  emission on the northeastern edge of the disk correlates with the outflow seen in  $^{12}\text{CO}(1-0)$  by Walter et al. (2002) and outlines the eastern edge of the hot gas associated with the outflow seen in diffuse X-rays (Stevens et al. 2003). The contours start at  $6\sigma$  and go up by factors of 2 ( $1\sigma_{\text{HCN}}=3.09 \text{ K km s}^{-1}$  and  $1\sigma_{\text{HCO}^+}=2.26 \text{ K km s}^{-1}$ ). The magenta ellipse in the top left panel indicates the region from which the spectra in Figure 2 were extracted. *Bottom Row:* The first moment map (mean velocity) for HCN,  $\text{HCO}^+$ , and  $^{12}\text{CO}(1-0)$ . Both velocity fields are consistent with a rotating torus of molecular material (Nakai et al. 1987; Shen & Lo 1995). The possibly outflowing  $\text{HCO}^+$  material north and south of the disk has velocities similar to the outflowing material in the center of M82 instead of velocities associated with the rotating molecular torus. The GBT, OVRO, and VLA beams are shown in the lower left corner of relevant panels and a  $10''$  scale-bar in the lower right hand corner of all panels.

ilar to the mode of the values found for other galaxies, while the  $L_{\text{CO}}/L_{\text{HCO}^+}$  value is slightly lower. The  $L_{\text{CO}}/L_{\text{HCN}}$  and  $L_{\text{CO}}/L_{\text{HCO}^+}$  values increase with distance from the center of the galaxy (bottom panels of Figure 3), suggesting the fraction of dense gas decreases with distance from the center. The  $L_{\text{HCN}}/L_{\text{HCO}^+}$  ratio is roughly constant across the center of the galaxy with higher values at the southern edge.

Figure 4 compares the relationship between the total molecular gas mass ( $L_{\text{CO}}$ ), the dense gas mass ( $L_{\text{HCN}}$  and  $L_{\text{HCO}^+}$ ), and the star formation rate ( $L_{\text{IR}}$ ) for the

entire M82 disk, points within M82, the sample of galaxies from the literature used in Figure 3, and star-forming regions in the Milky Way (Wu et al. 2010; Ma et al. 2012). We have estimated  $L_{\text{IR}}$  for the M82 points by multiplying the 3.0 GHz continuum flux density per pixel by the ratio of the infrared luminosity to the 3 GHz flux density for the entire galaxy. In effect, this procedure relies on the radio-infrared correlation, one of the tightest astronomical correlations, but avoids additional systematic errors by using the empirical ratio rather than a fit to the correlation seen in a large sample of galaxies. The use

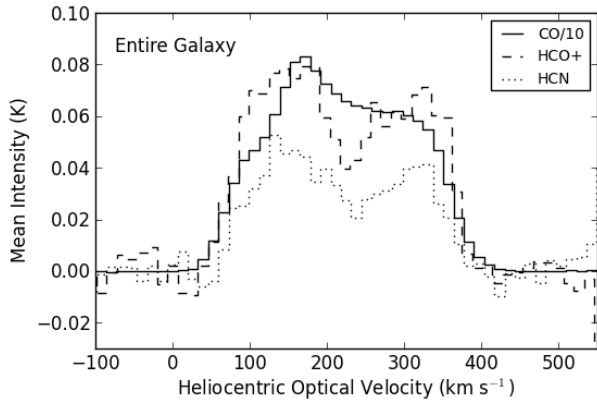


FIG. 2.— Mean intensity averaged over the disk of M82 for  $^{12}\text{CO}(2-1)$  (Leroy et al., in prep), HCN, and  $\text{HCO}^+$ . The region averaged is shown as a magenta ellipse in top left panel of Figure 1. The CO intensity has been divided by 10.

of the 3 GHz radio continuum ameliorates the significant optical depth effects found in edge-on galaxies like M82.

For the entire M82 disk, the relationship between the  $L_{\text{IR}}$  and  $L_{\text{HCN}}$  values matches the trend between  $L_{\text{IR}}$  and  $L_{\text{HCN}}$  found for a sample of LIRGs and ULIRGs, which have high star formation rates. However, our data shows that the relationship between  $L_{\text{IR}}$  and  $L_{\text{HCN}}$  varies *within* M82. Regions away from the central starburst tend to have lower  $L_{\text{IR}}$  (star formation rate) for a given amount of  $L_{\text{HCN}}$  (dense molecular gas). These points match the trend seen in normal galaxies (Gao & Solomon 2004b) and individual star-forming regions in the Milky Way (Wu et al. 2010). For points near the central starburst, the  $L_{\text{IR}}$  (star formation rate) is higher for a given amount of  $L_{\text{HCN}}$  (dense molecular gas), matching the trend seen for LIRG/ULIRGs. We see a similar trend for the  $\text{HCO}^+$  measurements. Compared to normal galaxies, individual regions in M82 tend to have higher dense gas fractions ( $L_{\text{HCN}}/L_{\text{CO}}$  or  $L_{\text{HCO}^+}/L_{\text{CO}}$ ) and higher ratios of star formation to total molecular gas mass ( $L_{\text{IR}}/L_{\text{CO}}$ ), but the dense gas fractions vary by a factor of 10.

These resolved observations of M82 show that the relationship between the amount of dense gas and star formation rate (as traced by the radio continuum) varies within a single galaxy. The key variable appears to be the central starburst, which could be using up or expelling the dense gas, affecting the gas tracer chemistry,

and/or changing how star formation proceeds. Future resolved observations of HCN and  $\text{HCO}^+$  in star-forming regions in a variety of galactic environments will allow us to disentangle these possibilities and understand how the central starburst in M82 influences star formation.

#### 4. SUMMARY

We have made the most sensitive map to date of the dense molecular gas in the starburst galaxy M82 using the largest single-dish millimeter-wave telescope in the world: the GBT. The HCN and  $\text{HCO}^+$  emission correlates with lower density molecular gas, traced by CO, and star formation, traced by radio continuum, and its kinematics are consistent with the previously proposed torus of molecular gas. We also detect low surface brightness  $\text{HCO}^+$  emission coincident with the base of the molecular gas outflow first detected in CO and tracing the edge of the hot outflowing gas seen in the X-ray.

The  $L_{\text{CO}}/L_{\text{HCN}}$ ,  $L_{\text{CO}}/L_{\text{HCO}^+}$ , and  $L_{\text{HCN}}/L_{\text{HCO}^+}$  ratios are similar to those in other starburst galaxies. The first two ratios increase with distance from the central starburst, implying that the fraction of dense gas decreases with distance from the starburst.

The relationship between the dense molecular gas and star formation varies with distance from the central starburst. Near its center, there is a higher ratio of star formation to dense molecular gas, similar to the relationship seen for LIRGs and ULIRGs, but outside of the central starburst, the ratio of the star formation to dense molecular gas decreases, agreeing with the correlation seen in normal galaxies and the Milky Way.

These observations demonstrate the effectiveness of the GBT for mapping dense molecular gas in external galaxies. The already-exciting capabilities of the GBT will be increased further with the advent of the 16 element 4mm feed array (ARGUS) being built for the GBT and will complement on-going efforts with ALMA.

The National Radio Astronomy Observatory is a facility of the National Science Foundation operated under cooperative agreement by Associated Universities, Inc. This research used APLpy and Astropy (The Astropy Collaboration et al. 2013).

*Facilities:* GBT, VLA

#### REFERENCES

- Aalto, S., García-Burillo, S., Muller, S., Winters, J. M., van der Werf, P., Henkel, C., Costagliola, F., & Neri, R. 2012, *A&A*, 537, A44
- Bolatto, A. D., Warren, S. R., Leroy, A. K., Walter, F., Villeux, S., Ostriker, E. C., Ott, J., Zwaan, M., Fisher, D. B., Weiss, A., Rosolowsky, E., & Hodge, J. 2013, *Nature*, 499, 450
- Brouillet, N., & Schilke, P. 1993, *A&A*, 277, 381
- Carilli, C. L., & Walter, F. 2013, *ARA&A*, 51, 105
- Dalcanton, J. J., Williams, B. F., Seth, A. C., Dolphin, A., Holtzman, J., Rosema, K., Skillman, E. D., Cole, A., Girardi, L., Gogarten, S. M., Karachentsev, I. D., Olsen, K., Weisz, D., Christensen, C., Freeman, K., Gilbert, K., Gallart, C., Harris, J., Hodge, P., de Jong, R. S., Karachentseva, V., Mateo, M., Stetson, P. B., Tavares, M., Zaritsky, D., Governato, F., & Quinn, T. 2009, *ApJS*, 183, 67
- Fuente, A., García-Burillo, S., Usero, A., Gerin, M., Neri, R., Faure, A., Le Bourlot, J., González-García, M., Rizzo, J. R., Alonso-Albi, T., & Tennyson, J. 2008, *A&A*, 492, 675
- Gao, Y., & Solomon, P. M. 2004a, *ApJS*, 152, 63
- . 2004b, *ApJ*, 606, 271
- García-Burillo, S., Usero, A., Alonso-Herrero, A., Graciá-Carpio, J., Pereira-Santaella, M., Colina, L., Planesas, P., & Arribas, S. 2012, *A&A*, 539, A8
- Graciá-Carpio, J., García-Burillo, S., Planesas, P., Fuente, A., & Usero, A. 2008, *A&A*, 479, 703
- Heiderman, A., Evans, II, N. J., Allen, L. E., Huard, T., & Heyer, M. 2010, *ApJ*, 723, 1019
- Juneau, S., Narayanan, D. T., Moustakas, J., Shirley, Y. L., Bussmann, R. S., Kennicutt, Jr., R. C., & Vanden Bout, P. A. 2009, *ApJ*, 707, 1217
- Kainulainen, J., Beuther, H., Henning, T., & Plume, R. 2009, *A&A*, 508, L35
- Krips, M., Neri, R., García-Burillo, S., Martín, S., Combes, F., Graciá-Carpio, J., & Eckart, A. 2008, *ApJ*, 677, 262
- Lada, C. J., Forbrich, J., Lombardi, M., & Alves, J. F. 2012, *ApJ*, 745, 190

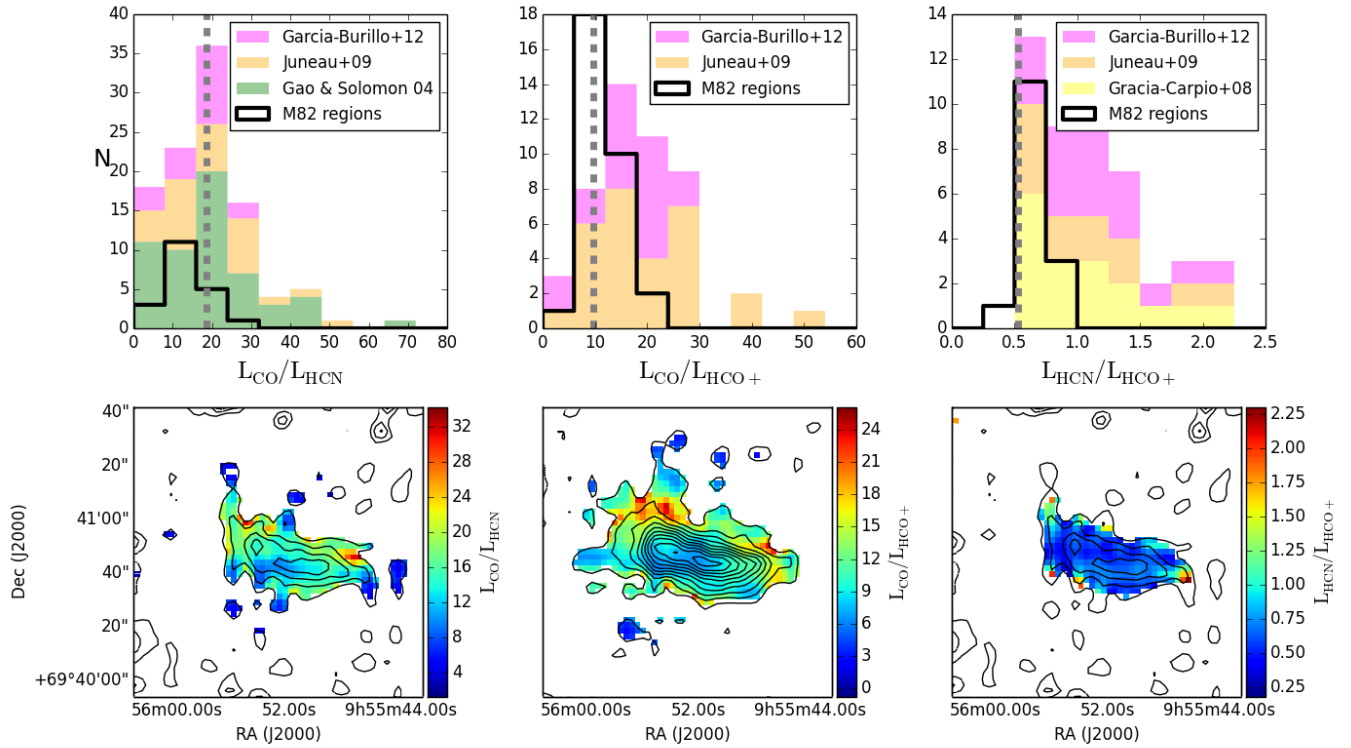


FIG. 3.— *Top*: The distributions of  $L_{CO}/L_{HCN}$  (left),  $L_{CO}/L_{HCO^+}$  (middle), and  $L_{HCN}/L_{HCO^+}$  (right) for regions in our M82 data compared to values for entire galaxies or galaxy centers from the literature (Gao & Solomon 2004b; Graciá-Carpio et al. 2008; Juneau et al. 2009; García-Burillo et al. 2012). For M82, only ratios with S/N greater than 6 are shown. The ratios between the total values for each quantity for M82 are shown as dashed gray lines. The ratios for M82 are similar to those seen in the literature, although the M82 distributions peak at lower ratios than the bulk of the literature values. *Bottom*: Spatial distribution of the  $L_{CO}/L_{HCN}$  (left),  $L_{CO}/L_{HCO^+}$  (middle), and  $L_{HCN}/L_{HCO^+}$  (right) ratios with the HCN (left and right) and  $HCO^+$  (middle) contours from Figure 1. The  $L_{CO}/L_{HCN}$  and  $L_{CO}/L_{HCO^+}$  values increase away from the center of the galaxy reflecting a decrease in dense gas away from the center of the starburst. The  $L_{HCN}/L_{HCO^+}$  ratio is constant across the face of the galaxy with slightly higher values found in the southern half of the galaxy.

Lada, C. J., Lombardi, M., & Alves, J. F. 2010, *ApJ*, 724, 687  
 Leroy, A. K., Walter, F., Sandstrom, K., Schruba, A., Munoz-Mateos, J.-C., Bigiel, F., Bolatto, A., Brinks, E., de Blok, W. J. G., Meidt, S., Rix, H.-W., Rosolowsky, E., Schinnerer, E., Schuster, K.-F., & Usero, A. 2013, *AJ*, 146, 19  
 Loenen, A. F., van der Werf, P. P., Güsten, R., Meijerink, R., Israel, F. P., Requena-Torres, M. A., García-Burillo, S., Harris, A. I., Klein, T., Kramer, C., Lord, S., Martín-Pintado, J., Röllig, M., Stutzki, J., Szczerba, R., Weiß, A., Philipp-May, S., Yorke, H., Caux, E., Delforge, B., Helmich, F., Lorenzani, A., Morris, P., Philips, T. G., Risacher, C., & Tielens, A. G. G. M. 2010, *A&A*, 521, L2  
 Ma, B., Tan, J. C., & Barnes, P. J. 2012, *ArXiv e-prints*  
 Maddalena, R. J. 2010, Theoretical Ratio of Beam Efficiency to Aperture Efficiency, GBT Memo 276, National Radio Astronomy Observatory  
 Mangum, J. G., Emerson, D. T., & Greisen, E. W. 2007, *A&A*, 474, 679  
 Nakai, N., Hayashi, M., Handa, T., Sofue, Y., Hasegawa, T., & Sasaki, M. 1987, *PASJ*, 39, 685  
 Nguyen-Q-Rieu, Nakai, N., & Jackson, J. M. 1989, *A&A*, 220, 57  
 Rieke, G. H., Lebofsky, M. J., Thompson, R. I., Low, F. J., & Tokunaga, A. T. 1980, *ApJ*, 238, 24

Sequist, E. R., Frayer, D. T., & Bell, M. B. 1998, *ApJ*, 507, 745  
 Shen, J., & Lo, K. Y. 1995, *ApJ*, 445, L99  
 Stevens, I. R., Read, A. M., & Bravo-Guerrero, J. 2003, *MNRAS*, 343, L47  
 The Astropy Collaboration, Robitaille, T. P., Tollerud, E. J., Greenfield, P., Droettboom, M., Bray, E., Aldcroft, T., Davis, M., Ginsburg, A., Price-Whelan, A. M., Kerzendorf, W. E., Conley, A., Crighton, N., Barbary, K., Muna, D., Ferguson, H., Grollier, F., Parikh, M. M., Nair, P. H., Günther, H. M., Deil, C., Woillez, J., Conseil, S., Kramer, R., Turner, J. E. H., Singer, L., Fox, R., Weaver, B. A., Zabalza, V., Edwards, Z. I., Azalee Bostroem, K., Burke, D. J., Casey, A. R., Crawford, S. M., Dencheva, N., Ely, J., Jenness, T., Labrie, K., Lian Lim, P., Pierfederici, F., Pontzen, A., Ptak, A., Refsdal, B., Servillat, M., & Streicher, O. 2013, *ArXiv e-prints*  
 Walter, F., Weiss, A., & Scoville, N. 2002, *ApJ*, 580, L21  
 Wu, J., Evans, II, N. J., Shirley, Y. L., & Knez, C. 2010, *ApJS*, 188, 313

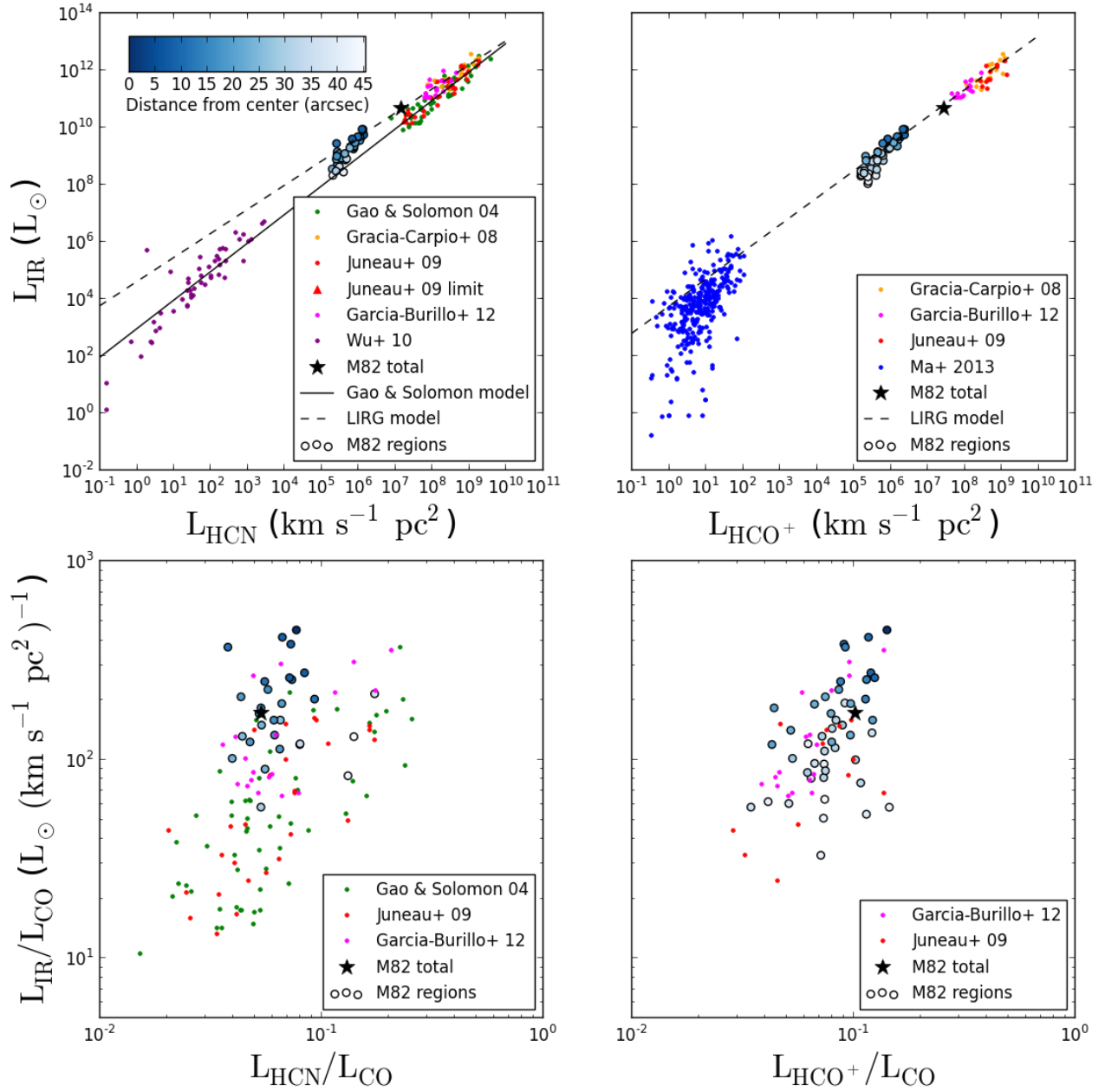


FIG. 4.— *Top:* The star formation rate traced by infrared luminosity as a function of the amount of dense gas traced by HCN (left) and HCO<sup>+</sup> (right). The  $L_{\text{IR}}\text{-}L_{\text{HCN}}$  fit for a sample including both normal galaxies and LIRGs/ULIRGs from Gao & Solomon (2004a) is shown as a solid line; star-forming regions within the Milky Way also follow this fit (Wu et al. 2010; Ma et al. 2012). The dotted line shows the  $L_{\text{IR}}\text{-}L_{\text{HCN}}$  fit derived from the sample of LIRGs/ULIRGs (Graciá-Carpio et al. 2008; García-Burillo et al. 2012). The integrated  $L_{\text{IR}}$  and  $L_{\text{HCN}}$  points for M82 follow the LIRG/ULIRG relationship between  $L_{\text{IR}}$  and  $L_{\text{HCN}}$ . Regions within M82, however, span a range of values with the high luminosity HCN and HCO<sup>+</sup> points following the LIRG/ULIRG relationship and the low luminosity points following instead the relationship seen in normal galaxies and in the Milky Way. We see a similar trend for  $L_{\text{IR}}$  vs.  $L_{\text{HCO}^+}$ . *Bottom:* In M82, the amount of dense gas per total molecular gas mass ( $L_{\text{HCN}}/L_{\text{CO}}$  and  $L_{\text{HCO}^+}/L_{\text{CO}}$ ) and the amount of star formation per total molecular gas mass ( $L_{\text{IR}}/L_{\text{CO}}$ ) are both high. The errors on the M82 data in all plots are smaller than the symbol size.